AIAA JOURNAL
Vol. 35, No. 2, February 1997

Low-Dispersion Finite Volume Scheme for Aeroacoustic Applications

Douglas V. Nance*
U.S. Air Force Wright Laboratory, Eglin Air Force Base, Florida 32542-6810
K. Viswanathan†
Dynacs Engineering Company, Inc., Renton, Washington 98055
and
L. N. Sankar‡
Georgia Institute of Technology, Atlanta, Georgia 30332

The development of a low-dispersion numerical scheme is described in the context of a finite volume discretization of the governing fluid dynamic equations. Although low-dispersion finite difference schemes have been developed recently for uniform Cartesian meshes, current finite volume methods do not possess low-dispersion characteristics. A low-dispersion finite volume scheme is presented and applied to some common acoustics problems. The two-dimensional unsteady Euler equations linearized about a mean flow are solved using a finite volume formulation. The surface integrals are computed using flow properties at cell faces, interpolated from cell nodes. The interpolation process is chosen such that it accurately represents sinusoidal waves of short wavelengths at the cell faces. A number of classical acoustics problems are solved, and where possible, comparisons with other numerical and exact solutions are given. This scheme has low dispersion and may be retrofitted easily into existing finite volume codes. The resulting numerical method combines the flexibility and versatility of the finite volume method while minimizing numerical dispersion errors in a manner similar to that of the classical dispersion-relation-preserving scheme.

Nomenclature

A, B	= flux Jacobian matrices
a_k	= stencil coefficients
C_v	= specific heat at constant volume
e	= total energy per unit mass
$\boldsymbol{E}$, $\boldsymbol{G}$	= flux vectors
F	= numerical flux at a cell side
H	= total enthalpy per unit mass
$\hat{\boldsymbol{i}}$, $\hat{\boldsymbol{j}}$	= Cartesian unit vectors
M_x, M_y	= main flowfield Mach numbers in the x and y directions
$\hat{\boldsymbol{n}}$	= unit normal vector
P	= pressure
$\boldsymbol{q}$	= vector-valued flow or acoustic variable
$\boldsymbol{q}_{L,R}$	= left or right upwind variable
r	= radial coordinate or stencil increment ratio
S	= surface enclosing a flow cell
T	= matrix transpose operator
t	= time-like variable
u	= x velocity or an acoustic variable
V	= flow cell volume
v	= y velocity
x, y	= Cartesian coordinates
α	= wave number
γ	= ratio of specific heats
ξ, η	= computational plane coordinates
ρ	= density
ω	= angular frequency

Introduction

THE mathematical common ground that exists between the fields of fluid dynamics and acoustics has motivated researchers to apply the techniques of computational fluid dynamics (CFD) to aeroacoustics problems. As a result, the 1980s saw the genesis of computational aeroacoustics (CAA). The first applications of CAA addressed problems such as hard-body scattering and sound-wave diffraction at sharp edges (e.g., Ref. 1) using classic CFD techniques. As pointed out by Hardin,[2] to facilitate the numerical resolution of the acoustic field, it is beneficial to regard acoustic properties as perturbations imposed upon an unsteady mean flowfield. This process yields a system of small-disturbance equations, hyperbolic in nature, that may be solved by using central difference schemes, the MacCormack method, or modern upwind schemes. Recent CAA techniques have been applied to aeroacoustic problems such as high-speed propeller noise,[3] cavity noise,[4] and jet noise.[5] Tam[6] provided a detailed discussion of the issues that are pertinent to aeroacoustics and outlined the stringent requirements necessary for applying numerical schemes in CAA applications.

Numerical dissipation and numerical dispersion are two primary sources of error associated with computational schemes. Because of these errors, traditional numerical schemes have been found to be unsatisfactory for the study of wave propagation over long distances and large time intervals. For example, pressure fluctuations associated with an intense acoustic wave are three orders of magnitude smaller than typical turbulent pressure fluctuations. Excessive numerical errors can overwhelm the small acoustic quantities of interest.[7] Therefore, these errors must be minimized. Specifically, dissipation causes a gradual decrease in the amplitude of an acoustic wave, particularly on coarse grids. Some researchers have advocated the use of a Kirchhoff approach to avoid the use of large computational domains and thus reduce dissipation.[8] On the other hand, dispersion causes waves of different wavelengths (or frequencies) to propagate at slightly different speeds. As a result, the traveling-wave profile may distort in a numerically induced, nonphysical manner. In addition to developing excellent radiation and outflow boundary conditions for use in CAA, Tam and Webb[9] have shown that if a given computational scheme and the governing equations have the same dispersion relations, then the numerical and exact solutions will have the same wave propagation characteristics and wave speeds. Accordingly, Tam and Webb developed the classic dispersion-relation-preserving (DRP) scheme, a new, optimized, high-order finite difference scheme that essentially preserves the wave propagation characteristics of the governing equations. The

Presented as Paper 96-0278 at the AIAA 34th Aerospace Sciences Meeting, Reno, NV, Jan. 15–18, 1996; received Jan. 29, 1996; revision received Nov. 1, 1996; accepted for publication Nov. 11, 1996; also published in *AIAA Journal on Disc*, Volume 2, Number 2.

*Research Scientist. Member AIAA.
†Member, Technical Staff. Member AIAA.
‡Professor, School of Aerospace Engineering. Senior Member AIAA.

classic DRP scheme is implemented by using a symmetric finite difference stencil on a uniform Cartesian grid. In this environment, the classic DRP schemes minimize numerical dispersion errors while producing essentially no dissipation errors. Unfortunately, practical problems in aeroacoustics are seldom confined to Cartesian geometries while the associated computational grids are nonuniform. As a result, the classic DRP approach is often not desirable for use. Still, in practical problems, the acoustic field consists predominantly of high-frequency waves that are especially sensitive to phase and damping errors. For this reason, numerical dissipation and dispersion must be controlled in CAA solvers.

Motivation for Present Work

The objective of the present study is to develop a low-dispersion finite volume (LDFV) scheme for aeroacoustic applications. As discussed in the Introduction, the classic DRP scheme of Tam and Webb[9] has superior dispersion characteristics, but, to date, has been applied only on Cartesian, uniformly spaced grids. The proposed approach will try to mimic many of the features of the classic DRP scheme in a curvilinear, finite volume framework. A direct application of DRP methodology to the finite volume formulation is difficult, because the former scheme tries to model spatial derivatives such as $\partial u/\partial x$ and $\partial v/\partial y$, as accurately as possible. In finite volume schemes, on the other hand, these derivatives get converted into surface integrals involving u and v, etc. Thus, the most that can be hoped for is the representation of u and v, etc., as accurately as possible on the finite volume cell faces. For example, let us consider the continuity equation

$$\frac{\partial \rho}{\partial t} + \frac{\partial(\rho u)}{\partial x} + \frac{\partial(\rho v)}{\partial y} = 0 \Leftrightarrow \frac{\partial}{\partial t}\int\int_V \rho \,\mathrm{d}V + \oint_S \rho \boldsymbol{v} \cdot \hat{\boldsymbol{n}} \,\mathrm{d}S = 0$$

In the classical DRP scheme, the derivatives on the left side of this equivalence relation are discretized. As a result, the derivatives of ρu and ρv will be represented in such a way as to match the dispersion relation for $\partial/\partial x$ or $\partial/\partial y$, as necessary. On the other hand, the proposed LDFV scheme uses optimized interpolation formulas for ρ, u, v, and P on a given cell face. This scheme is designed to accurately match the dispersion relation for the actual properties on the computational stencil, not their gradients. For linear problems, the interpolation procedure is modified to operate on the linearized flux variables. It is unclear whether this approach will automatically lead to low dispersion. The concepts of dispersion and dissipation are well developed in finite difference schemes but less well developed for finite volume schemes. The finite volume technique facilitates easy modeling of complex geometries such as airfoils, wings, bodies, and propellers, whereas the quasi-DRP features of this new approach ensure numerically accurate solutions. The current LDFV method is tested in both new and preexisting computer programs. Several benchmark problems considered in a recent Institute for Computer Applications in Science and Engineering/NASA Langley Research Center (ICASE/LaRC) workshop[10] on CAA are solved. The numerical results are compared with exact solutions and with solutions computed by other numerical schemes. This paper is organized as follows: The mathematical formulation is described first. Some of the methods of achieving low dispersion are explored and the attendant limitations are discussed. Finally, results of some validation studies are presented.

Mathematical and Numerical Formulation

Governing Acoustic Equations

The governing equations are written in two dimensions for the sake of simplicity, but the methods developed below may be extended easily to three dimensions. The Euler equations are best suited for the study of both linear and nonlinear acoustics because viscosity plays a negligible role as far as acoustics are concerned.[11] We can write the Euler equations for a calorically perfect gas as

$$\frac{\partial \boldsymbol{q}}{\partial t} + \frac{\partial \boldsymbol{F}}{\partial x} + \frac{\partial \boldsymbol{G}}{\partial y} = 0 \tag{1}$$

where

$$\begin{aligned} \boldsymbol{q} &= (\rho, \rho u, \rho v, \rho e)^T \qquad e = C_v T + \tfrac{1}{2}(u^2 + v^2) \\ \boldsymbol{F} &= (\rho u, \rho u^2 + P, \rho u v, \rho u H)^T \\ \boldsymbol{G} &= (\rho v, \rho u v, \rho v^2 + P, \rho v H)^T \qquad H = e + (P/\rho) \end{aligned} \tag{2}$$

Consider the vector of conserved variables $\boldsymbol{q}$. We can decompose each component of this vector into the sum of its mean flow and acoustic constituents,[2,3] i.e.,

$$\boldsymbol{q} = \boldsymbol{q}_0 + \boldsymbol{q}' \tag{3}$$

where the subscript 0 indicates the unsteady main flow and the primed quantity represents the acoustic fluctuation. The equation set for the acoustic perturbations can be written as

$$\frac{\partial \boldsymbol{q}'}{\partial t} + \frac{\partial(A\boldsymbol{q}')}{\partial x} + \frac{\partial(B\boldsymbol{q}')}{\partial y} = 0 \tag{4}$$

where A and B are the flux Jacobian matrices for $\boldsymbol{F}$ and $\boldsymbol{G}$, respectively. The mean flow equations are solved first, and the perturbation equations (4) are solved in the second step. This procedure is adopted for all the numerical schemes considered.

Temporal Discretization

Both the finite difference and finite volume solutions of either equation set (1) or (4) ultimately require integration of the following ordinary differential equation:

$$\frac{\partial \boldsymbol{q}'}{\partial t} = \boldsymbol{R} \tag{5}$$

Equation (5) is numerically integrated in time by using the two-step Runge–Kutta scheme

$$\begin{aligned} \boldsymbol{q}'^{p} &= \boldsymbol{q}'^{n} + \Delta t \boldsymbol{R}^{n} \\ \boldsymbol{q}'^{(n+1)} &= \tfrac{1}{2}(\boldsymbol{q}'^{n} + \boldsymbol{q}'^{p}) + (\Delta t/2)\boldsymbol{R}^{p} \end{aligned} \tag{6}$$

The quantity $\boldsymbol{R}$ can be computed in a number of ways. We first examine how this is done in a finite volume scheme.

Finite Volume Method

In a finite difference scheme, the numerical solution is computed at a finite set of points, usually the grid points or nodes. The finite volume solution is computed in a set of cells that are in some way associated with the grid points. The cells have volume, or area in the case of two dimensions. The properties of $\boldsymbol{q}_0$ and $\boldsymbol{q}'$ should be viewed as average properties within these cells. This discretization procedure is different from that of the finite difference method. Let us begin with the hyperbolic set of equations (4). If we integrate this equation over a cell volume in a two-dimensional flowfield and apply the divergence theorem, we obtain

$$\frac{\partial}{\partial t}\int\int_V \boldsymbol{q}' \,\mathrm{d}V + \oint_S (\hat{\boldsymbol{A}}\boldsymbol{i} + \hat{\boldsymbol{B}}\boldsymbol{j})\boldsymbol{q}' \cdot \hat{\boldsymbol{n}} \,\mathrm{d}S = 0 \tag{7}$$

The first term in Eq. (7) contains the integral of $\boldsymbol{q}'$ over the cell area. The second term in Eq. (7) represents the transport of flux across cell boundaries. For quadrilateral cells, we can discretize the second term in Eq. (7) as follows:

$$R_{i,j} = \sum_{m}^{4} \bar{F}^{m}_{i,j} = \sum_{m}^{4} [(\hat{\boldsymbol{A}}\boldsymbol{i} + \hat{\boldsymbol{B}}\boldsymbol{j})\boldsymbol{q}' \cdot \hat{\boldsymbol{n}} \,\Delta S]^{m}_{i,j} \tag{8}$$

where index m denotes the sides of cell (i, j). The various finite volume schemes differ in the way the numerical flux $\bar{F}^{m}_{i,j}$ is evaluated. We now drop the subscript i, j and the superscript m for convenience. For two-dimensional cells, consider the cell interface AB given in Fig 1.

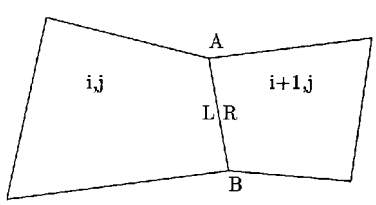

Fig. 1 Finite volume cell interface.

MacCormack's Scheme

In the MacCormack[12] scheme, $\boldsymbol{F}$ is computed using $\boldsymbol{q}_L$, where $\boldsymbol{q}$ is estimated using information from the left side (L) of cell face AB during the predictor stage of the Runge–Kutta scheme. In the corrector stage, $\boldsymbol{F}$ is computed using $\boldsymbol{q}_R$, estimated at the right side (R) of the cell face AB. Here $\boldsymbol{q}$ refers to both the mean flow variables $\boldsymbol{q}_0$ and acoustic variables $\boldsymbol{q}'$.

Central Difference Scheme

In a central difference approach, made popular by Jameson et al.,[13] $\boldsymbol{F}$ is computed using an algebraic average of $\boldsymbol{q}_L$ and $\boldsymbol{q}_R$. Two popular choices are

$$\bar{F} = \boldsymbol{F}\left(\frac{\boldsymbol{q}_L + \boldsymbol{q}_R}{2}\right) \tag{9}$$

and

$$\bar{F} = \tfrac{1}{2}[\boldsymbol{F}(\boldsymbol{q}_L) + \boldsymbol{F}(\boldsymbol{q}_R)] \tag{10}$$

Upwind Scheme

In this approach, $\boldsymbol{F}$ is split into flux vectors $\bar{\boldsymbol{F}}^+$ and $\bar{\boldsymbol{F}}^-$, associated with waves that travel out of and into the cell, respectively. Then,

$$\bar{F} = \bar{\boldsymbol{F}}^+(\boldsymbol{q}_L) + \bar{\boldsymbol{F}}^-(\boldsymbol{q}_R) \tag{11}$$

This approach was used by Steger and Warming[14] and by Van Leer.[15] For the CAA equations, this approach was proposed by Sankar et al.[16]

Low-Dispersion–High-Accuracy Estimates for $\boldsymbol{q}_L$ and $\boldsymbol{q}_R$

Thus far, we have not specified how $\boldsymbol{q}_L$ and $\boldsymbol{q}_R$ should be computed. As an example, consider the two-dimensional cell with grid coordinates i, j given in Fig. 1. Consider the choice:

$$\boldsymbol{q}_L = \boldsymbol{q}_{i,j}; \qquad \boldsymbol{q}_R = \boldsymbol{q}_{i+1,j} \tag{12}$$

In an upwind scheme, however, this choice will lead only to a first-order scheme. Higher-order monotone upwind-centered schemes for conservation laws (MUSCL) interpolation will improve formal spatial accuracy, as suggested by Van Leer.[17] The proposed scheme seeks $\boldsymbol{q}_L$ and $\boldsymbol{q}_R$ estimates that not only will lead to high spatial accuracy, but low dispersion. To achieve this goal, we first examine Tam's classic DRP scheme applied to the one-dimensional analog of Eq. (1):

$$\frac{\partial \boldsymbol{q}'}{\partial t} + \frac{\partial \bar{F}}{\partial x} = 0$$

Classic DRP Scheme

Here we present a brief discussion of Tam's classic DRP scheme for the purpose of comparison with the LDFV scheme. A thorough treatment of the DRP finite difference scheme may be found in Tam and Webb.[9] For the purpose of illustration, we select a centrally symmetric discretization on a uniform grid for $\partial \boldsymbol{F}/\partial x$, i.e.,

$$\frac{\partial \boldsymbol{F}_i}{\partial x} = \frac{1}{\Delta x}\sum_{k=-M}^{M} a_k \boldsymbol{F}_{i+k} \tag{13}$$

where the coefficients a_k are fixed in all space and for all time. Our goal is to choose these coefficients so as to minimize the dispersion error inherent in the right-hand side of Eq. (13). We begin by taking the Fourier integral transform of Eq. (13) to obtain

$$i\alpha\Delta x = \sum_{k=-M}^{M} a_k \exp(ik\alpha\Delta x) \tag{14}$$

or we can write

$$\overline{\alpha\Delta x} = -i\sum_{k=-M}^{M} a_k \exp(ik\alpha\Delta x) \tag{15}$$

where $\overline{\alpha\Delta x}$ is the numerical wave number/mesh-size product.[9] Because of simplifications rendered by the use of a uniform grid, we have written the numerical $\overline{\alpha\Delta x}$ in terms of its actual value $\alpha\Delta x$. Tam proposed to select the coefficients a_k such that $\overline{\alpha\Delta x}$ closely matches $\alpha\Delta x$ over the wave-number range of interest. We can accomplish this task in a least-squares sense. The classic DRP minimization equations are given by

$$\frac{\partial}{\partial a_j}\left[\int_{-\pi/2}^{\pi/2} \left\|\overline{\alpha\Delta x} - \alpha\Delta x\right\|^2 \mathrm{d}(\alpha\Delta x)\right] = 0, \qquad j = -M, \ldots, M \tag{16}$$

Typically, a relation from the minimization procedure is solved along with a set of Taylor-series equations developed for $\partial \boldsymbol{F}/\partial x$. The Taylor-series-based equations maintain the required order of accuracy while the minimization relation from Eq. (16) forces the system to match the dispersion relation for the first derivative. The end result is a symmetric difference formula meeting the desired requirements for accuracy and DRP behavior. Tam's DRP scheme performs very well for Cartesian finite difference applications but is not well suited for application on irregular geometries or with upwind schemes. In fact, the DRP method's limitations are associated with its uniform, symmetric differencing stencil. In most fluid or acoustic problems, the grid becomes quite nonuniform both in the field and adjacent to the boundaries. Uniform stencils are very difficult to implement in these areas, and they induce ambiguous representations of surface boundary conditions near a curved wall. Moreover, classic DRP stencils do not support upwinding because of their inherent symmetry. Our intent is to present a scheme with the desirable attributes of both DRP and upwind finite volume schemes.

Low-Dispersion Finite Volume Scheme

One way of achieving high spatial accuracy in a finite volume scheme is to compute $\boldsymbol{q}_L$ and $\boldsymbol{q}_R$ using high-order polynomial interpolation formulas for each component of the vector $\boldsymbol{q}$. The interpolation is carried out in a transformed plane (ξ, η), where the quadrilateral cells are mapped onto uniform squares. For example,

$$\begin{aligned} q_L &= q_i + \tfrac{1}{3}(q_{i+1} - q_i) + \tfrac{1}{6}(q_i - q_{i-1}) \\ q_R &= q_{i+1} - \tfrac{1}{6}(q_{i+1} - q_i) - \tfrac{1}{3}(q_{i+2} - q_{i+1}) \end{aligned} \tag{17}$$

This set of interpolants is known as the standard third-order MUSCL scheme.[3] Unfortunately, this approach leads to significant dispersion when applied to the CAA workshop problems.[10] For the LDFV method, we begin by establishing a stencil for $q_{i+1/2}$. The equations for our applications are developed in the uniform (ξ, η) plane. Suppose we use a general stencil for q, say,

$$q_{i+\frac{1}{2}} = \sum_{k=-M}^{N} a_k\, q(\xi_{+\frac{1}{2}} + \Delta_k\xi) \tag{18}$$

where $\Delta_k\xi$ is a set of $(M + N)$ constant parameters based on the grid-point spacing $\Delta\xi$. Note that we can control the direction of upwinding in the stencil by changing the positive integers M and N. We can take the Fourier transform of Eq. (18) with $\xi_{+1/2}$ as the variable of integration. Hence,

$$Q(\alpha\Delta\xi) = \sum_{k=-M}^{N} a_k \exp(i\alpha\Delta_k\xi) \tag{19}$$

By the exact Fourier transform, Eq. (19) becomes unity. In this case, we can write $\Delta_k\xi$ in terms of the uniform stepsize $\Delta\xi$, i.e.,

$$\Delta_k\xi = \beta_k\Delta\xi$$

where

$$\beta_k \in \left\{\ldots, -\tfrac{5}{2}, -\tfrac{3}{2}, -\tfrac{1}{2}, \tfrac{1}{2}, \tfrac{3}{2}, \tfrac{5}{2}, \ldots\right\}$$

Therefore,

$$Q(\alpha\Delta\xi) = \sum_{k=-M}^{N} a_k \exp(i\beta_k\,\alpha\Delta\xi) \tag{20}$$

and this sum also can be expressed as a function of the wave number/mesh-size product $\alpha\Delta\xi$. To preserve the dispersion relation for q, the real part of Eq. (20) must equal one. Accordingly,

we use least squares to determine the expansion coefficients. With $\phi = \alpha\Delta\xi$, let us minimize the quantity

$$E(a_j) = \int_{-\pi/2}^{\pi/2} \left\| 1 - \sum_{k=-M}^{N} a_k e^{i\beta_k\phi} \right\|^2 d\phi \qquad (21)$$

subject to the coefficients a_k. Obtaining the minimization relations is a straightforward exercise, i.e.,

$$\frac{\partial E(a_k)}{\partial a_j} = 0, \qquad j = -M, \ldots, N \qquad (22)$$

Equation (22) produces $(M + N)$ equations in terms of the unknowns a_j. The numerical problems described in this work were solved with coefficients created by combining one minimization equation from Eq. (22) with $(M + N - 1)$ equations taken from Taylor-series expansions.

Let us consider the LDFV analog of Eq. (17), an asymmetric three-point formula. We require three equations to solve for the coefficients, two from the Taylor-series expansions for, say, $q_{i+1/2}$. The remaining equation is chosen from system (22). Because there are three minimization equations, we obtain three possible sets of coefficients. If we substitute the coefficients into Eq. (20) and examine its real and imaginary parts, we can study the dispersive and dissipative performance of the scheme. The real part represents dispersion whereas the imaginary part represents dissipation.[8] Asymmetric formulas are characterized by the presence of nonzero real and imaginary parts. Figure 2 contains the dispersion curves $Re[F(q_{i+1/2})]$ for the three- and five-point LDFV formulas. Curves for a set of nonoptimized three- and five-point formulas are shown for comparison. These curves indicate that, in the sense of dispersion, our optimized numerical scheme performs better than contemporary upwind schemes. Figure 3 contains the imaginary dissipation curves $Im[F(q_{i+1/2})]$ for the same LDFV formulas. This plot shows that the asymmetric LDFV formulas are subject to dissipation more so than current upwind schemes. We can write a general three-point interpolation formula as follows:

$$q_{i+\frac{1}{2}} = a_{-1}q_{i-1} + a_1 q_i + a_2 q_{i+1} \qquad (23)$$

For the third-order MUSCL scheme (17), the coefficients a_k are

$$a_{-1} = -0.1667; \qquad a_1 = 0.8333; \qquad a_2 = 0.3333$$

For the second-order low-dispersion system, the coefficients in Eq. (23) are given as

$$a_{-1} = -0.1128; \qquad a_1 = 0.7257; \qquad a_2 = 0.3872$$

Clearly, the low-dispersion optimization procedure has perceptibly altered the interpolation scheme. This result is interesting and useful; others may desire to try it on their problems of interest.

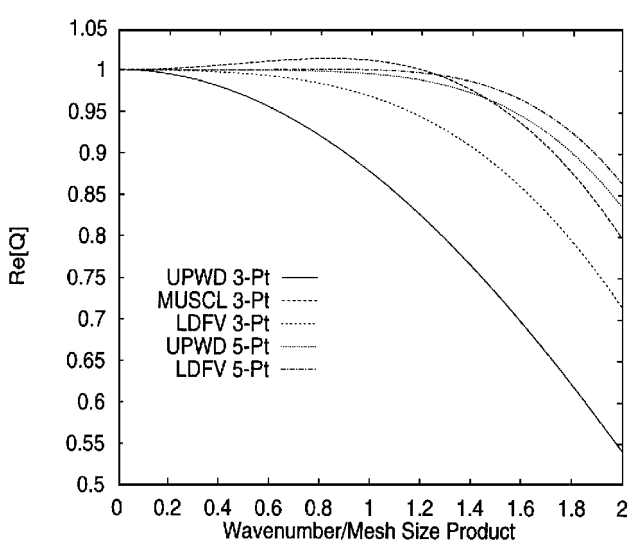

Fig. 2 Real dispersion curves.

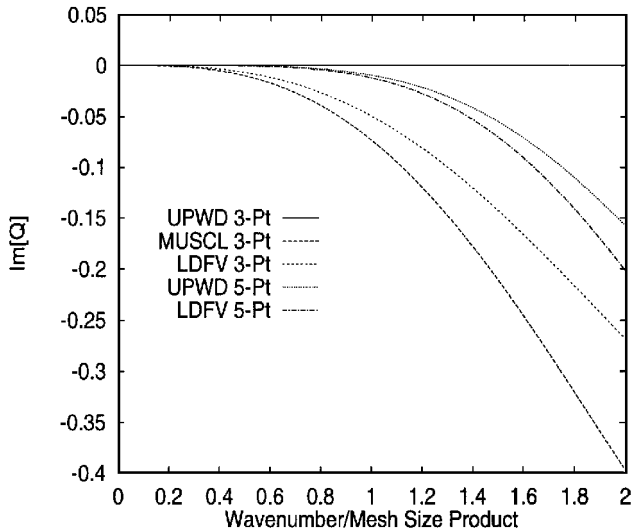

Fig. 3 Imaginary dissipation curves.

Higher-Order Low-Dispersion Schemes

We can logically extend our method of interpolation to higher orders. The codes tested in the analyses below incorporate a five-point interpolation scheme. Our upwind scheme requires left and right interpolants, so we use the interpolation formulas

$$q_L = q^L_{i+\frac{1}{2}} = q_i + b_L(q_{i-1} - q_{i-2}) + c_L(q_i - q_{i-1}) + d_L(q_{i+1} - q_i) + e_L(q_{i+2} - q_{i+1}) \qquad (24)$$

$$q_R = q^R_{i+\frac{1}{2}} = q_{i+1} - b_R(q_i - q_{i-1}) - c_R(q_{i+1} - q_i) - d_R(q_{i+2} - q_{i+1}) - e_R(q_{i+3} - q_{i+2}) \qquad (25)$$

The optimization procedure is unchanged, but the algebra is more complicated. The five-point system incorporating Eqs. (24) and (25) can be analyzed by plotting the real and imaginary parts of the expression

$$Q(\alpha\Delta\xi) = \sum_{j=-3}^{3} a_j \exp(i\alpha\Delta_j\xi) \qquad (26)$$

Recalling that ideally $Q(\alpha\Delta\xi)$, the coefficients a_j can be obtained easily with the optimization procedure. The $\Delta_j\xi$ are given by the stencil. In this case,

$$\Delta_{-2}\xi = -\tfrac{5}{2}\Delta\xi; \qquad \Delta_{-1}\xi = -\tfrac{3}{2}\Delta\xi; \qquad \Delta_1\xi = -\tfrac{1}{2}\Delta\xi;$$
$$\Delta_2\xi = \tfrac{1}{2}\Delta\xi; \qquad \Delta_3\xi = \tfrac{3}{2}\Delta\xi$$

The coefficients in Eqs. (24) and (25) are selected to yield a fourth-order LDFV scheme. The order of accuracy for the LDFV scheme is given by the algebraic order of the upwind variables q_L or q_R. In contrast, the order of accuracy for a MUSCL scheme is given by the algebraic order of the difference[17]:

$$q_R - q_L$$

Figures 2 and 3 contain the real (dispersion) curve and the imaginary (dissipation) curve, respectively, for this system. Figure 3 demonstrates that the low-dispersion interpolation matches the dispersion relation better than the Taylor-series expansion. In many cases like those presented in Fig. 3, the optimized interpolation stencil is more dissipative than the Taylor stencil. The low-dispersion stencil does possess the negative dissipation sometimes found in asymmetric stencils, indicative of a possible instability. In fact, asymmetric formulas tend to be unstable even when used for solving linear differential equations. Usually, schemes containing asymmetric formulas require some numerical damping. The dispersive and dissipative behavior depicted in Figs. 2 and 3 is commonly found in the comparison of basic upwind schemes with LDFV schemes. In general, the LDFV scheme of order n will have less dispersion but more dissipation than a basic upwind scheme of order $n + 1$ when computed on the same stencil.

Table 1 Comparison of coefficients of five-point LDFV and UPWD formulas

a_k	LDFV	UPWD
a_{-2}	0.0299695	0.0234375
a_{-1}	−0.182378	−0.15625
a_1	0.742317	0.703125
a_2	0.442622	0.46875
a_3	−0.0325305	−0.0390625

High-Order Limiter

High-order interpolations (24) and (25), and the corresponding MUSCL interpolations, work well for smooth variations of $\boldsymbol{q}$. For nonlinear problems, near discontinuities in the numerical solution, high-order interpolation may cause nonphysical oscillations. A limiter that locally reduces the interpolation to first order is then required. For the development of a high-order limiter, we may follow Van Leer[17] or Hirsch.[18] Our interpolating polynomials now appear as

$$q_L = q_i + b_L\Phi^+_{i-\frac{3}{2}}(q_{i-1} - q_{i-2}) + c_L\Phi^+_{i-\frac{1}{2}}(q_i - q_{i-1}) + d_L\Phi^-_{i+\frac{1}{2}}(q_{i+1} - q_i) + e_L\Phi^-_{i+\frac{3}{2}}(q_{i+2} - q_{i+1}) \tag{27}$$

$$q_R = q_{i+1} - b_R\Phi^+_{i-\frac{1}{2}}(q_i - q_{i-1}) - c_R\Phi^+_{i+\frac{1}{2}}(q_{i+1} - q_i) - d_R\Phi^-_{i+\frac{3}{2}}(q_{i+2} - q_{i+1}) - e_R\Phi^-_{i+\frac{5}{2}}(q_{i+3} - q_{i+2}) \tag{28}$$

where Φ is some limiter function meeting the total variation diminishing (TVD) requirements outlined by Sweby.[19] Also, we can specify the limiter functions in terms of their arguments, e.g.,

$$\Phi^+_{i-\frac{1}{2}} = \Phi\left(r^+_{i-\frac{1}{2}}\right); \qquad \Phi^-_{i+\frac{1}{2}} = \Phi\left(r^-_{i+\frac{1}{2}}\right) \tag{29}$$

where

$$r^+_{i-\frac{1}{2}} = \frac{q_{i+1} - q_i}{q_i - q_{i-1}}; \qquad r^-_{i+\frac{1}{2}} = \frac{q_i - q_{i-1}}{q_{i+1} - q_i} \tag{30}$$

The other ratios of form (30) can be found by shifting the index i. Roe's Superbee limiter function is used in Eq. (29) for solving our test-case problems.[17] The Superbee limiter function is given by

$$\Phi(r) = \max[0, \min(2r, 1), \min(r, 2)] \tag{31}$$

Naturally, other limiter functions can be used in this scheme as long as they satisfy the TVD requirements. For completeness, the LDFV and UPWD five-point formula coefficients are compared in Table 1. This limiter efficiently removes unwanted oscillations from our numerical solutions without excessively damping acoustic waves present in the solution.

Validation Studies

Four problems were chosen for the validation process. The first three were selected from the ICASE/LaRC Workshop test cases.[10] This reference specifies and defines a detailed spatial mesh separately for each problem. We have not diverged from these specifications. A classic acoustics problem, the scattering of a plane wave by a cylinder, has been chosen for validating our methods on an arbitrary geometry. A two-step Runge–Kutta time integration scheme has been used in each case, and all calculations have been performed using a Silicon Graphics R3000 workstation.

Problem 1: Spherical Wave Equation

Recall that the spherical wave equation has the form

$$\frac{\partial u}{\partial t} + \frac{u}{r} + \frac{\partial u}{\partial r} = 0, \qquad r > 5, \qquad t > 0 \tag{32}$$

In this case, Eq. (32) is solved with the time-dependent boundary condition

$$u = 5\cos(\omega t), \qquad r = 5, \qquad t > 0$$

where

$$\omega = \pi/4$$

The radial grid is uniform with $\Delta r = 1$, and the time integration step size is $\Delta t = 0.01$. The solution was calculated for Eq. (32) using conservative and nonconservative forms. The results are essentially identical in each case. The asymmetric finite volume formulas proved to be unstable for use in this problem. The centered formula for $u_{i+1/2}$ was stable and produced good results. Figures 4 and 5 contain the solution plots for times $t = 100$ and 200. The $t = 100$ solution was calculated in 113 CPU seconds. In both cases, the exact and numerical solutions agree suitably, except the numerical solution becomes more dispersive with time. Dispersion, in this case, manifests itself through the lagging in time of the numerical solution behind the exact solution. Also, we can observe dissipation in the propagating wave. The solution is smeared and damped at large times. A close examination of Figs. 4 and 5 shows that our LDFV solution performs decidedly better than the standard third-order MUSCL scheme. Moreover, our solution is comparable to both the exact solution and to a fourth-order MacCormack scheme.[20] Unlike their asymmetric counterparts, the centered finite volume formulas are quite stable when advanced in time. Still, the asymmetric formulas prove to be suitable for use in upwind schemes.

Problem 2: Nonlinear Acoustic Pulse

This test case requires the numerical solution of an initial value problem using the Euler equations in one dimension. These

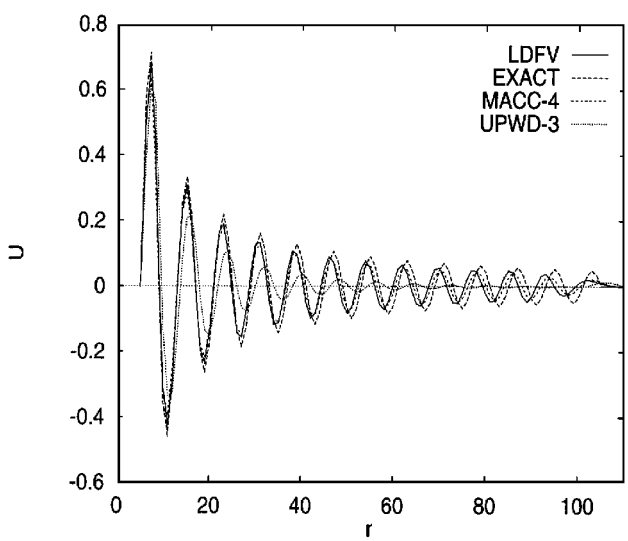

Fig. 4 Spherical wave equation T = 100.

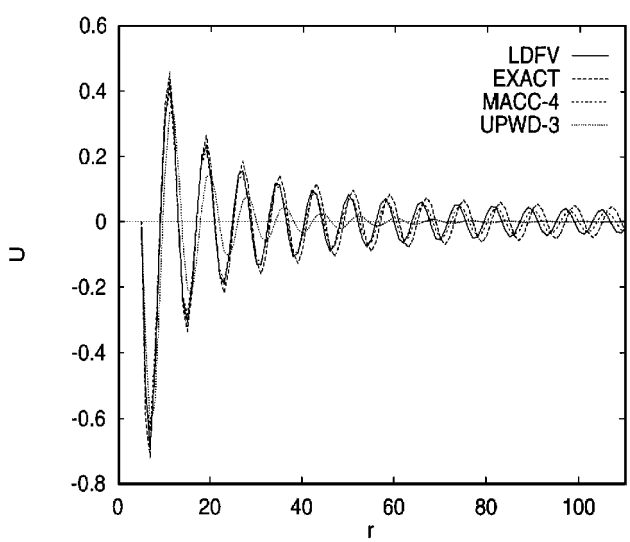

Fig. 5 Spherical wave equation T = 200.

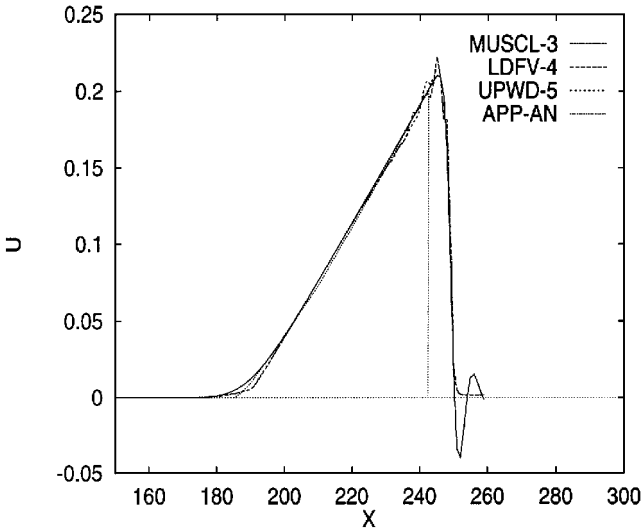

Fig. 6 Nonlinear pulse problem $T = 200$.

equations can be obtained by setting $G = v = 0$ in Eq. (1). The flowfield properties are initialized as follows at time $t = 0$:

$$u(x) = \tfrac{1}{2}\exp[-\ln(2)(x/5)^2]$$

$$P(x) = (1/\gamma)\{1 + [(\gamma - 1)/2]u(x)\}^{2\gamma/(\gamma-1)}$$

$$\rho(x) = \{1 + [(\gamma - 1)/2]u(x)\}^{2/(\gamma-1)}$$

A uniform grid is established on a segment of the x axis with $\Delta x = 1$. Also, nonreflecting boundary conditions are implemented at the left and right ends of this segment. Roe's flux difference splitting scheme is used for spatial integration in conjunction with our high-order limiter given in Eqs. (29) through (31). The solution evolves with a fixed time step of 0.01 and is shown for time $t = 200$ in Fig. 6. The numerical solution (LDFV-4) is compared with an approximate analytical method (APP-AN) produced by Whitham's kinematic wave method.[21] It also is compared with the third-order MUSCL scheme (MUSCL-3) and with a fifth-order upwind scheme (UPWD-5). No limiter is used with the MUSCL scheme, and all results are quite good. Our proposed scheme captures the trailing portion of the shock more sharply than the MUSCL scheme and equally as well as the fifth-order scheme. The LDFV solution also captures the leading shock front well, predicting a stronger shock than the MUSCL scheme. Near the shock-wave peak, the LDFV solution has fewer overshoots than the fifth-order solution. The MUSCL solution also displays a pronounced oscillation at the shock front. Numerical experiments have shown that this oscillation can be removed by the use of a limiter, but the resulting solution is severely degraded by dissipation. All three of these numerical schemes predict a broader shock profile than is shown by the approximate analytical method. However, this characteristics-based method may not capture the true thickness of the shock because of the highly nonlinear behavior of the flow near the discontinuity. The LDFV solution requires 1004 CPU seconds, whereas the MUSCL solution requires 877 CPU seconds. So, in the light of increased accuracy and dispersion matching behavior, the added computing time is a reasonable investment for this problem.

Problem 3: Reflection of an Acoustic Pulse in a Uniform Flow Off a Wall

This problem entails a solution of the linearized Euler equations in two dimensions. The governing equations are given by Eq. (1) with the substitutions

$$\boldsymbol{q} = (\rho, u, v, p)^T; \qquad \boldsymbol{F} = \begin{bmatrix} M_x\rho + u \\ M_x u + p \\ M_x v \\ M_x p + u \end{bmatrix}; \qquad \boldsymbol{G} = \begin{bmatrix} M_y\rho + v \\ M_y u \\ M_y v + p \\ M_y p + v \end{bmatrix} \tag{33}$$

The symbols M_x and M_y are the mean-flow Mach numbers in the x and y directions. The acoustic pulse is initialized as a two-dimensional Gaussian pulse centered at $x = 0$, $y = 25$. There is a solid wall at $y = 0$. For purposes of code validation, we consider $M_x = 0.5$ and $M_y = 0$. The numerical pulse shapes are compared to the exact solution on a 201×201 grid. Because this problem entails only linear acoustics, our fourth-order low-dispersion scheme, Eqs. (24) and (25), was used to compute a solution. The LDFV-4 solution requires 4291 CPU seconds, whereas the sixth-order MacCormack solution[10] requires 2018 CPU seconds, so the use of the LDFV scheme requires twice the computer time for this problem. This numerical solution is compared with both the MacCormack solution and with the third-order MUSCL solution. Our LDFV solution is compared with both the sixth-order MacCormack and third-order upwind solutions in Figs. 7–10. There is excellent agreement with the exact solution over the smoother regions of the pulse. In some instances, the LDFV solver performs better than the standard upwind scheme near the pulse peaks. However, the dissipation inherent in this scheme is evident near the pulse extrema.

Problem 4: Scattering of Plane Wave by a Cylinder

In this two-dimensional test case, an plane acoustic wave of unit wave number and unit propagation speed scatters off of a rigid circular cylinder of radius 0.1. The simple polar grid selected for this problem begins with a wall spacing of 0.025. The grid evolves radially

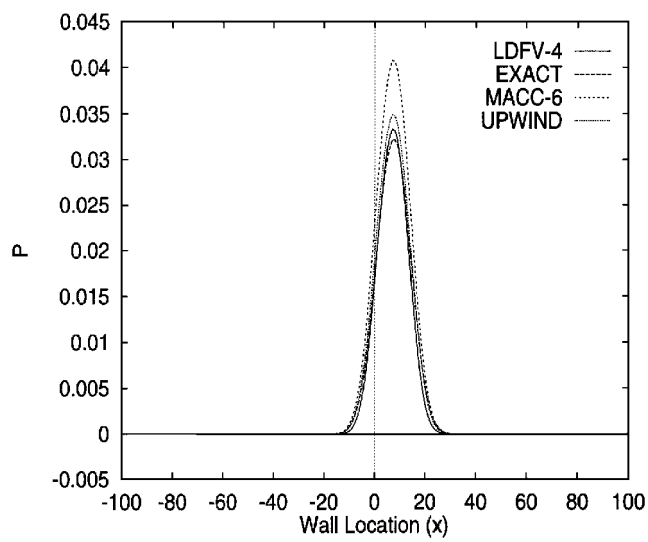

Fig. 7 Wall-reflected pulse solution $T = 15$.

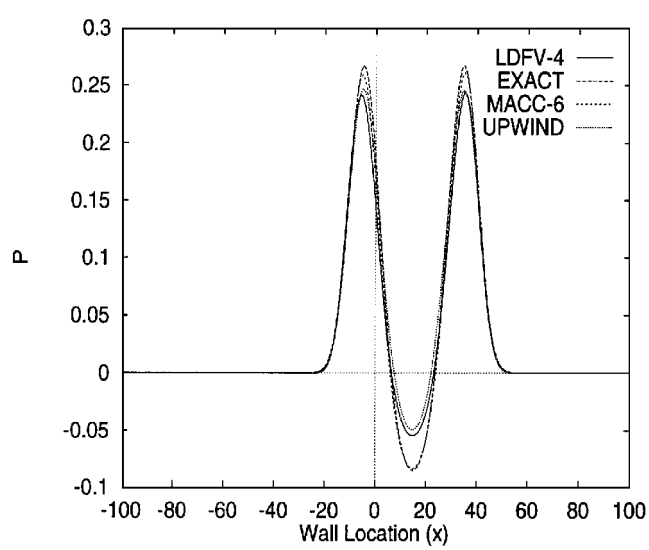

Fig. 8 Wall-reflected pulse solution $T = 30$.

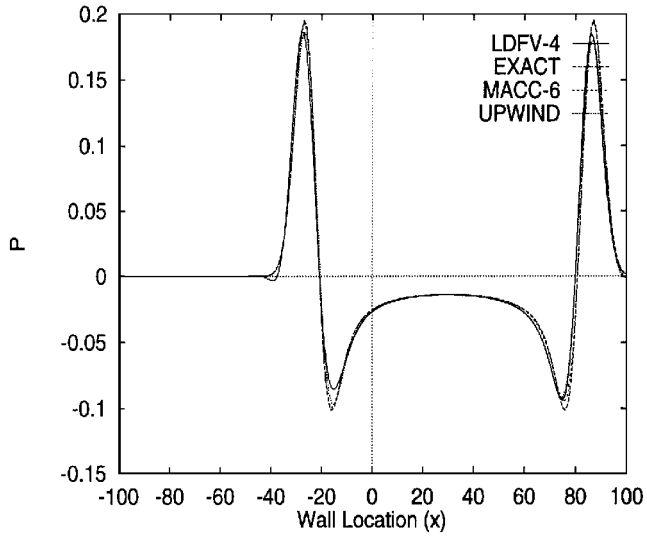

Fig. 9 Wall-reflected pulse solution $T = 60$.

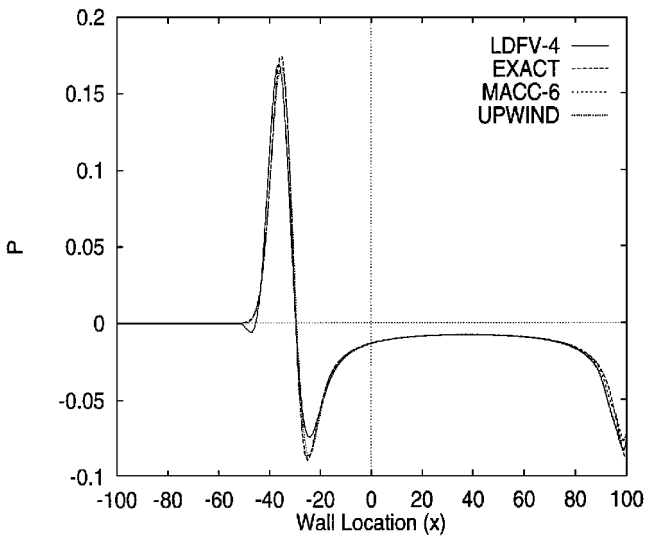

Fig. 10 Wall-reflected pulse solution $T = 75$.

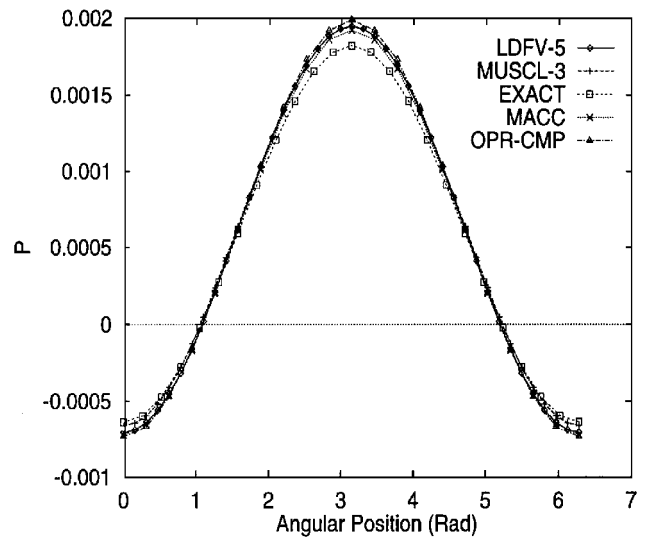

Fig. 11 Acoustic pressure at $R = 1$, time = 17.2.

with $\Delta r = 0.025$ until one-half of the radial points are generated. Then the grid spreads radially with the ratio

$$\frac{\Delta r^{k+1}}{\Delta r^{k}} = 1.1$$

until the outer boundary is reached. The azimuthal grid maintains a fixed angular increment of $\Delta\theta = \pi/20$. Nonreflecting boundary

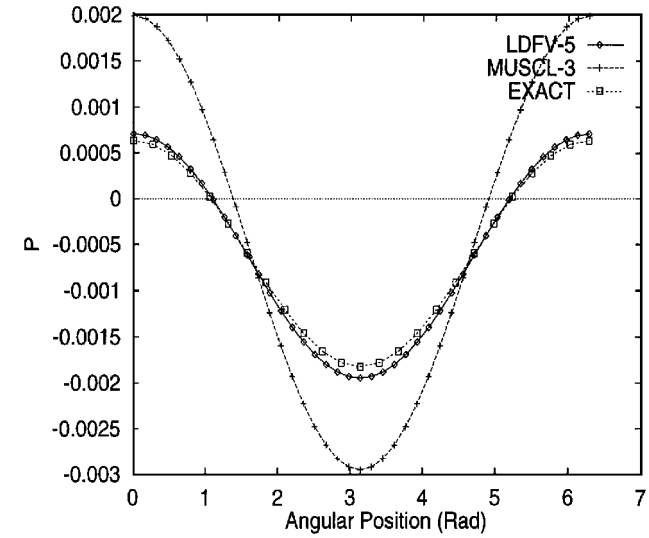

Fig. 12 Acoustic pressure at $R = 1$, time = 14.1.

conditions are implemented at the outer boundary, and the time step is fixed at 0.01. In Fig. 11, the LDFV-4 pressure solution for the scattered acoustic wave is plotted at time $t = 11\pi/2$. It is compared with a set of numerical solutions rendered by other methods and with the exact solution.[22] The performance of the LDFV-4 solution is clearly comparable with that of the finite difference schemes. As is evidenced in Fig. 12, a comparative solutions plot at time $t = 9\pi/2$, the LDFV-4 solutions frequently perform better than the third-order MUSCL solution. Both upwind methods require about 1280 CPU seconds to render a time $t = 6\pi$ solution. The accuracy of upwind schemes tends to vary depending on the solution time. Our scheme also tends to be less dissipative than the MUSCL scheme. Similar behavior can be seen on differing polar grids.

Concluding Remarks

A new upwind, finite volume scheme has been developed for use in CAA solvers. It incorporates some of the features of the classic DRP scheme for controlling dispersion in the numerical solution. The current versions of the scheme are second- and fourth-order accurate in space and second-order accurate in time. A limiter is incorporated in the scheme for removing unwanted nonphysical oscillations from the numerical solutions of nonlinear problems.

This finite volume scheme has been validated through the numerical solution of several problems taken from classic sources as well as from the recent workshop on CAA. Our low-dispersion finite volume solutions have obtained acceptable agreement with available exact analytical solutions. Most existing finite volume codes can be retrofitted with the present scheme simply through the replacement of their current expressions for q_L and q_R with our proposed low-dispersion formulas.

An improved version of this scheme that has a lower dissipation level is now under development by the first author. In this approach, a low dispersion approximation for $q_R - q_L$ is first found, before q_L and q_R are extracted for use as upwind variables. The results of this approach will be published elsewhere.

References

[1]Khan, M. M. S., "Computational Aeroacoustics Applied to Diffraction of Sound by Cylindrical Bodies," *AIAA Journal*, Vol. 25, No. 7, 1987, pp. 949–956.

[2]Hardin, J., Lecture, Forum on Computational Aeroacoustics and Hydroacoustics, American Society of Mechanical Engineers, June 1993.

[3]Lim, T. B., Sankar, L. N., Hariharan, N., and Reddy, N. N., "A Technique for the Prediction of Propeller-Induced Acoustic Loads on Aircraft Surfaces," AIAA Paper 93-4340, 1993.

[4]Hardin, J. C., and Pope, S. D., "Sound Generation by Flow over a Two-Dimensional Cavity," *AIAA Journal*, Vol. 33, No. 3, 1995, pp. 407–412.

[5]Viswanathan, K., and Sankar, L. N., "Toward the Direct Calculation of Noise: Fluid/Acoustic Coupled Simulation," *AIAA Journal*, Vol. 33, No. 12, 1995, pp. 2271–2279.

[6]Tam, C. K. W., "Computational Aeroacoustics: Issues and Methods," *AIAA Journal*, Vol. 33, No. 10, 1995, pp. 1788–1796.

[7]Hardin, J., "Regarding Numerical Considerations for Computational Aeroacoustics," *Computational Aeroacoustics*, Springer–Verlag, New York, 1993, pp. 216–228.

[8]Lyrintzis, A. S., "Review: The Use of Kirchhoff's Method in Computational Aero- and Hydroacoustics," *Journal of Fluids Engineering*, Vol. 116, 1994, pp. 665–676.

[9]Tam, C. K. W., and Webb, J. C., "Dispersion-Relation-Preserving Schemes for Computational Aeroacoustics," *Journal of Computational Physics*, Vol. 107, 1993, pp. 262–281.

[10]Hardin, J. C., Ristorcelli, J. R., and Tam, C. K. W. (eds.), *Proceedings of the ICASE/LaRC Workshop on Benchmark Problems in Computational Aeroacoustics (CAA)*, CP-3300, NASA, 1995.

[11]Pierce, A. D., *Acoustics: An Introduction to Its Physical Principles and Applications*, Acoustical Society of America, New York, 1991.

[12]MacCormack, R. W., "The Effect of Viscosity in Hypervelocity Impact Cratering,," AIAA Paper 69-354, 1969.

[13]Jameson, A., Schmidt, W., and Turkel, E., "Numerical Simulation of the Euler Equations by Finite Volume Methods Using Runge–Kutta Time Stepping Schemes," AIAA Paper 81-1259, 1981.

[14]Steger, J. L., and Warming, R. F., "Flux Vector Splitting of the Inviscid Gas-Dynamic Equations with Applications to Finite Difference Methods," *Journal of Computational Physics*, Vol. 40, 1981, pp. 263–293.

[15]Van Leer, B., "Flux Vector Splitting for the Euler Equations," *Proceedings of the Eighth International Conference on Numerical Methods in Fluid Dynamics*, Springer–Verlag, Berlin, 1982.

[16]Sankar, L. N., Reddy, N. N., and Hariharan, N., "A Third Order Upwind Scheme for Aero-Acoustic Applications," AIAA Paper 93-0149, 1993.

[17]Van Leer, B., "Towards the Ultimate Conservative Difference Scheme, V: A Second Order Sequel to Godunov's Method," *Journal of Computational Physics*, Vol. 32, 1979, pp. 101–136.

[18]Hirsch, C., *Numerical Computation of Internal and External Flows*, Vol. 2, Wiley, New York, 1990.

[19]Sweby, P. K., "High Resolution Schemes Using Flux Limiters for Hyperbolic Conservation Laws," *SIAM Journal on Numerical Analysis*, Vol. 21, No. 5, 1984, pp. 995–1011.

[20]Gottlieb, D., and Turkel, E., "Dissipative Two-Four Methods for Time-Dependent Problems," *Mathematics of Computation*, Vol. 30, No. 136, 1976, pp. 703–723.

[21]Whitham, G. B., *Linear and Nonlinear Waves*, Wiley, New York, 1974.

[22]Morse, P. M., *Vibration and Sound*, Acoustical Society of America, New York, 1936.